Syntheses, crystal, molecular structures, and solution studies of Cu(II), Co(II), and Zn(II) coordination compounds containing pyridine-2,6-dicarboxylic acid and 1,4-pyrazine-2,3-dicarboxylic acid: comparative biological studies of Cu(II), Al, and Zn(II) complexes

M. Mirzaei, H. Eshtiagh-Hosseini, N. Alfi, H. Aghabozorg, J. Attar Gharamaleki, S. A. Beyramabadi, H. R. Khavasi, A. R. Salimi, A. Shokrollahi, et al.

 Springer

Springer

ORIGINAL RESEARCH

Syntheses, crystal, molecular structures, and solution studies of Cu(II), Co(II), and Zn(II) coordination compounds containing pyridine-2,6-dicarboxylic acid and 1,4-pyrazine-2,3-dicarboxylic acid: comparative computational studies of Cu(II) and Zn(II) complexes

M. Mirzaei · H. Eshtiagh-Hosseini · N. Alfi · H. Aghabozorg ·
J. Attar Gharamaleki · S. A. Beyramabadi · H. R. Khavasi ·
A. R. Salimi · A. Shokrollahi · R. Aghaei · E. Karami

Abstract Three new coordination compounds of Cu(II), Co(II), and Zn(II) based on different dicarboxylic acids formulated as $(AcrH)[Cu(pydc)(pydcH)]\cdot 5H_2O$ (**1**) $(2a\text{-}4mpyH)_2[M(pyzdc)_2(H_2O)_2]\cdot 6H_2O$; M = Co(II) (**2**) and Zn(II) (**3**) have been synthesized and structurally characterized by elemental analyses, IR spectroscopy, and single crystal X-ray diffraction (where $pydcH_2$ = pyridine-2,6-dicarboxylic acid; Acr = acridine; 2a-4mpy = 2-amino-4-methyl pyridine; $pyzdcH_2$ = 1,4-pyrazin-2,3-dicarboxylic acid). In all cases, the metal centers have distorted octahedral coordination geometries. Through

M. Mirzaei (✉) · H. Eshtiagh-Hosseini (✉) · N. Alfi ·
A. R. Salimi
Department of Chemistry, Ferdowsi University of Mashhad,
917751436 Mashhad, Iran
e-mail: mirzaeesh@ferdowsi.um.ac.ir

H. Eshtiagh-Hosseini
e-mail: heshtiagh@ferdowsi.um.ac.ir

H. Aghabozorg · J. A. Gharamaleki
Faculty of Chemistry, Tarbiat Moallem University, Tehran, Iran

S. A. Beyramabadi
Department of Chemistry, Faculty of Science, Islamic Azad
University, Mashhad Branch, Mashhad, Iran

H. R. Khavasi
Departement of Chemistry, Shahid Beheshti University,
G. C., Evin, 1983963113 Tehran, Iran

A. Shokrollahi · R. Aghaei · E. Karami
Department of Chemistry, Yasouj University, Yasouj, Iran

hydrogen bonding (such as O–H···O and N–H···O) and/or slipped or offset π–π stacking interactions, 3D supramolecular networks are constructed in these complexes. In the crystalline network, O–H···O hydrogen bonding create $(H_2O)_n$ water clusters, so the hydrogen bond interactions play an important role in sustaining of the supramolecular solid-state architectures in compounds **1**–**3**. The species in the solution media were studied by potentiometric method. The protonation constants of 2a-4mpy, 2-apy = 2-amino-pyridine, pydc and pyzdc in aqueous solution, pydc and Acr in a 50% dioxane–50% water (v/v) solvent, as well as the equilibrium constants for three proton-transfer systems, pyzdc-2a-4mpy, pydc-2-apy, and pydc-Acr were calculated using potentiometrical method. The stoichiometry and stability of complexation during the first proton-transfer system with Cu^{2+}, Co^{2+}, and Zn^{2+} ions and also the second proton-transfer system with Fe^{3+} and Cr^{3+} ions in aqueous solution were investigated by potentiometric pH titration method, from point of comparison view of their behaviors in the solution state. The stoichiometry and stability of complexation of third system with Cu^{2+} and Zn^{2+}, metal ions in 50% dioxane–50% water (v/v) solvent were also investigated by the cited method. The stoichiometry of the most complex species in solution were compared with corresponding crystalline metal ion complexes. Furthermore, DFT calculations have been carried out on the Cu(II) and Zn(II) complexes in the presence of $pydcH_2$ and $pyzdcH_2$ in order to better understanding of their molecular orbital structures of HOMO and LUMO.

Introduction

There is an increasing attention in transition metal coordination compounds with conjugated organic ligands bearing functional groups [1–11]. The complexes have diverse noncovalent interactions such as aromatic–aromatic stacking, donor–acceptor interactions, hydrogen bonding, etc. [12, 13]. The current interests are focused on the hydrogen bond aggregation to create supramolecular network. Hydrogen bonding has the strong directional effect to organize individual molecules into supramolecular aggregate. The classical hydrogen bonds formed by such carboxylics, amines, amids, hydroxyl, etc. Functional groups are widely employed to construct crystalline edifice [14, 15]. In this work, a systematic study was employed for proton-transfer process from carboxylic acids to amines [16–29]. PydcH$_2$ and pyzdcH$_2$ were used as ligands in designing coordination compounds with various dimensionalities and inducing self-assembly processes [30–42]. Due to interesting characteristics of pydcH$_2$ and pyzdcH$_2$, they are good candidate for the construction of supramolecular compounds. As valuable characters are: (a) heterocyclic acid with two carboxyl groups, (b) form hydrogen bonding and aromatic–aromatic stacking interactions, (c) contain N– or O– donor atoms, these leads to new structures with diverse dimensional. Previously, the syntheses and structural characterization of some coordination compounds via proton-transfer methodology were described [16–29]. Herein, the syntheses and potentiometric studies of three new Cu(II), Co(II), and Zn(II) coordination compounds involving abovementioned dicarboxylic acids as proton donors, and Acr and 2a-4mpy heterocyclic amines as proton acceptors are reported. The obtained coordination compounds have been characterized by CHN elemental analyses, IR spectroscopy, and single crystal X-ray diffraction method. In the following sections, the DFT studies on highest occupied molecular orbital (HOMO) and lowest unoccupied molecular orbital (LUMO) characteristics are also presented for Cu(II) and two Zn(II) [31] complexes bearing pydcH$_2$ and pyzdcH$_2$ ligands.

Experimental

Materials and physico-chemical measurements

All chemicals and solvents with reagent grade from Merck, used without further purification. Infrared spectra in the range of 4000–600 cm^{-1} were recorded on a Buck 500 scientific spectrometer using KBr disc. Elemental analysis was carried out with a Thermo Finnigan Flash-1112EA microanalyzer and Perkin-Elmer 2004(II) apparatus. The TG runs were taken on a TGA-50/50H standard type thermal analysis system. The compound was heated up to 1,000 °C in the atmosphere of nitrogen, with heating rate of 10 K per min.

Potentiometric equilibrium measurements

Equipment

A Model 794 Metrohm Basic Titrino was attached to an extension combined glass-calomel electrode mounted in an air-protected, sealed, thermostated jacketed cell, maintained at 25.0 ± 0.1 °C by circulating water, from a constant-temperature bath Fisher brand model FBH604, LAUDA, Germany, equipped with a stirrer and a 10,000-mL-capacity Metrohm piston burette. The pH meter-electrode system was calibrated to read −log [H$^+$] in water and for reading −log [H$^+$] in 50% dioxane–50% water (v/v) solvent.

Synthesis of (AcrH)[Cu(pydc)(pydcH)]·5H$_2$O (**1**)

To an aqueous solution containing pydcH$_2$ (0.33 g, 2.0 mmol) and Acr (0.18 g, 1.0 mmol) was added to solution of copper(II) nitrate hexahydrate (0.15 g, 0.50 mmol). The solution with total volume of 50 mL was stirred and heated very slightly. By slow cooling, suitable green prism crystals were obtained after 3 weeks. Anal. Calcd. for C$_{27}$H$_{27}$CuN$_3$O$_{13}$: C, 48.76; H, 4.09; N, 6.32. Found: C, 48.53; H, 3.94; N, 6.21%. IR data (cm^{-1}): 3200–3600(br), 3093(m), 2938(w), 1644(s), 1633(m), 1592(s), 1556(m), 1428(s), 1368(br), 1274(br), 1183(s), 1149(m), 1085(s), 1034(m), 900(s), 788(s), 739(s), 682(s), 601(m), 522(w), 462(m), 414(w), 337(w), 317(w).

Synthesis of (2a-4mpyH)$_2$[Co(pyzdc)$_2$(H$_2$O)$_2$]·6H$_2$O (**2**)

A solution of pyzdcH$_2$ (0.40 g, 0.24 mmol) in 10 mL water was added dropwise to a stirring solution at 90 °C, containing 2a-4mpy (0.15 g, 0.14 mmol). Then, a solution of CoCl$_2$·6H$_2$O (0.076 mmol, 13 mg) was added to above solution. Single crystals of **2** suitable for X-ray diffraction as orange block shape were obtained by slow evaporation of solvent at RT after half a day. Anal. Calcd. for C$_{24}$H$_{38}$CoN$_8$O$_{16}$: C, 38.1; H, 5.0; N, 14.9. Found: C, 38.2; H, 4.9; N, 14.9%. IR data (cm^{-1}): 3400(s), 3100(w), 1680(sh), 1650(w),1620(w), 1460(s),1380(vs), 1360(w), 1310(w), 1150(vs), 1065(m), 985(m), 940(m),895(s), 745(br), 445(s).

Synthesis of (2a-4mpyH)$_2$[Zn(pyzdc)$_2$(H$_2$O)$_2$]·6H$_2$O (**3**)

Similar to the preparation of **2**, the mixture of 2a-4mpy (0.050 g, 0.41 mmol) and pyzdcH$_2$ (0.040 g, 0.24 mmol) was refluxed for an hour. Then, solution of Zn(NO$_3$)$_2$·4H$_2$O

(0.020 g, 0.080 mmol) was added dropwise and refluxing continued for 6 h at 90 °C. After slow evaporation of solvent at RT block light pink crystals were collected. Anal. Calcd. for $C_{24}H_{38}ZnN_8O_{16}$: C, 37.8; H, 4.9; N, 14.7. Found: C, 38.2; H, 4.7; N, 14.7%. IR data (cm^{-1}): 3400(sh), 1660(w), 1640(w), 1620(w), 1570(sh), 1465(w), 1460(m), 1390, 1370 1310(sh), 1120(s), 990(m), 890(s), 840(s).

Synthesis of (2-apyH)[Fe(pydc)$_2$]·pydcH$_2$·5H$_2$O

A solution of 2-apy (0.030 g, 0.60 mmol) and pydcH$_2$ (0.010 g, 0.30 mmol) was refluxed for 1 h. Then solution of FeCl$_3$·6H$_2$O (0.080 g, 0.30 mmol) was added dropwise and refluxing continued for 6 h at 90 °C. After slow evaporation of solvent at RT light green block crystals were collected. Anal. Calcd. for $C_{26}H_{29}FeN_5O_{17}$: C, 42.2; N, 9.4. Found: C, 38.8; N, 10.2%. IR data (cm^{-1}): 3324(m), 3139(br), 3081(br), 2920(sh), 1680(vs), 1471(w), 1417(w), 1344(s), 12579(w), 1159(s), 1072(m), 984(w), 916(m),756(w).

Synthesis of (2-apyH)[Cr(pydc)$_2$]·pydcH$_2$·5H$_2$O

A solution of 2-apy (0.030 g, 0.60 mmol) and pydcH$_2$ (0.01 g, 0.30 mmol) was refluxed for 1 h. Then, a solution of CrCl$_3$·6H$_2$O (0.08 g, 0.30 mmol) was added dropwise and refluxing continued for 6 h at 90 °C. After slow evaporation of solvent at RT pure precipitation were collected. Anal. Calcd. for $C_{26}H_{29}CrN_5O_{17}$: C, 42.4, H, 3.9. Found: C, 47.4; H, 3.6%. IR data (cm^{-1}): 3414(m), 3087(w), 2500-2385(br),1660(vs), 1332(s), 1260(w), 1100(w), 753(w).

Crystal structure determination and structural refinement of coordination compounds 1–3

Single crystal data were collected on a Bruker SMART 1000 CCD area detector (compound **1**) and Stoe IPDS II diffractometer (compounds **2** and **3**) equipped with graphite-monochromated Mo K_α radiation. Empirical absorption corrections were employed. The structure was solved by SHELXTL [43–48]. The final refinement was done by full-matrix least squares based on F^2 with anisotropic thermal parameters for all non-hydrogen atoms, the hydrogen atoms of compound **1** were generated geometrically and for compounds **2** and **3** mixed method (geometrically and difference Fourier map). The crystal data and experimental conditions as well as the final parameters were summarized in Table 1. The selected bond lengths and angles together with the hydrogen bonding geometry were shown in Tables 2 and S1, respectively.

Results and discussion

Thermal gravimetric analysis

The thermal gravimetric analysis (TGA) of the synthesized complexes **2**, **3** as well as Fe(III),[1] Cr(III),[2] and Cu(II) complexes [24] for finding a good comparison were carried out in nitrogen atmosphere from 20 to 1,000 °C as shown in Fig. S1. The initial stage for **2**, 65–85 °C shows it losses the coordinated and non-coordinated water molecules (found: 18.0%, calcd.: 16.9%). The second stage corresponds to the loss of two (pyzdc)$^{2-}$ ligands and 2a-4mpy counter cation (found: 59%, calcd.: 58.6%). The final residue shows the cobalt oxide, CoO (found: 10%, calcd.: 9.95%). In **3**, there are three decomposition stages. The first stage of weight loss which begins at 50 °C and ends at 100 °C was attributed to the loss of coordinated and non-coordinated water molecules (found: 19%, calcd.: 18.94%). The second stage of weight loss is attributed to (pyzdc)$^{2-}$ ligand and counter cation (found: 60%, calcd.: 59.07%). The third stage corresponds to the thermal decomposition and complete destruction of the crystalline network producing ZnO (found: 15%, calcd.: 10.65%). The TGA study of Cu(II) coordination compounds [24] (which is isostructural with **2** and **3** counterpart) exhibits three steps of weight loss. At the first step, there is a 18% weight loss from 50 to 80 °C, which attributed to the loss of two coordinated water molecules together with three non-coordinated water molecules (calcd.: 16.06%). Anhydrous complex is stable up to 245 °C. In the second stage, Cu(II) compound begins to decompose between 245 and 285 °C and to calculate mass loss for two (pyzdc)$^{2-}$ ligands and (2a-4mpyH)$^+$ counter cation (calcd.: 74.19%). The total mass of decomposition process (found: 88%, calcd.: 89.27%) suggesting that CuO is the final product at 380 °C. Thermal analysis of Fe(III) shows that the first step starts at 220 °C with a weight loss of 30% and continues to 250 °C, which corresponds to the loss of five water molecules and one pydcH$_2$ (calcd.: 34.4%). The next weight loss occurred at 300–360 °C which belongs to decomposition of the anionic and the cationic fragments (found: 45%, calcd.: 43%). The final step of the crystalline network decomposition shows the formation of Fe$_2$O$_3$. For Cr(III) counterpart, the first stage at 260–320 °C range corresponds to the loss of the five crystallization water molecules and one pydcH$_2$ (found: 30.0, calcd.: 34.96%). The second stage, between 170 and 328 °C response to the decomposition of both cationic and anionic fragment (found: 52.0, calcd.: 58.0%). The third stage is related to the decomposition of

---

[1] We are now improving its X-ray data for future report.

[2] We are now trying to get suitable single crystal of this compound for X-ray crystallographic analysis.

Table 1 The summary of crystallographic data for compounds **1–3**

	1	**2**	**3**
Empirical formula	$C_{27}H_{27}CuN_3O_{13}$	$C_{24}H_{38}CoN_8O_{16}$	$C_{24}H_{38}ZnN_8O_{16}$
Formula weight	665.06	753.25	760.01
Temperature (K)	120(2)	298(2)	298(2)
Wavelength (Å)	0.71073	0.71073	0.71073
Crystal system	Monoclinic	Triclinic	Triclinic
Space group	$P2_1/n$ $Z = 4$	$P\bar{1}$ $Z = 1$	$P\bar{1}$ $Z = 1$
Unit cell dimensions	$a = 9.6595(17)$ Å	$a = 6.9452(15)$ Å	$a = 6.9456(7)$ Å
	$\alpha = 90.00°$	$\alpha = 80.001(18)°$	$\alpha = 79.581(7)°$
	$b = 18.884(4)$ Å	$b = 8.5012(18)$ Å	$b = 8.4762(8)$ Å
	$\beta = 97.464(7)°$	$\beta = 82.384(18)°$	$\beta = 82.901(8)°$
	$c = 15.512(3)$ Å	$c = 14.349(3)$ Å	$c = 14.4733(13)$ Å
	$\gamma = 90.00°$	$\gamma = 85.191(17)°$	$\gamma = 85.174(8)°$
Absorption coefficient (mm^{-1})	0.854	0.60	0.82
$F(000)$	1,372	393	396
θ range for data collection	1.7°–28°	2.4–29.3°	2.5–29.3°
Index ranges	$-12 \leq h \leq 12$	$-9 \leq h \leq 9$	$-9 \leq h \leq 9$
	$-23 \leq k \leq 24$	$-11 \leq k \leq 11$	$-11 \leq k \leq 11$
	$-20 \leq l \leq 20$	$-19 \leq l \leq 16$	$-19 \leq l \leq 19$
Reflections collected/ unique	22,069/6,753 [R(int) = 0.047]	9,777/4,419 [R(int)] = 0.078	10,071/4,454 [R(int) = 0.094]
Goodness-of-fit on F^2	1.00	1.142	1.027
Final R indices [$I > 2\sigma(I)$]	$R_1 = 0.0484$	$R_1 = 0.0405$	$R_1 = 0.0574$
	$wR_2 = 0.0899$	$wR_2 = 0.1330$	$wR_2 = 0.1491$
Largest diff. peak and hole	0.95 to -0.49 e $Å^{-3}$	0.38 to -0.45 e $Å^{-3}$	0.93 to -1.80 e $Å^{-3}$

crystalline network and production of Cr_2O_3 fragment (found: 11.0%, calcd.: 20.6%). The TGA result of Cr(III) indicates similar structure like that of Fe(III). It should be pointed out that the above evidences substantiate well the chemical structures which confirmed by single crystal X-ray analyses.

Structural description of compound **1**

The molecular structure of compound **1** is illustrated in Fig. 1. According to the crystal structures, the Cu(II) compound composed of monoanionic complexes, [Cu(pydc)(pydcH)]$^-$, acridinium ions as counter ion, (AcrH)$^+$ and five uncoordinated water molecules. In the crystal structure of the title compounds, the central atoms are coordinated by two tridentate (pydc)$^{2+}$ and (pydcH)$^-$ groups and the presence of an (AcrH)$^+$ ions, balance the negative charges. N1 and N2 atoms occupy the axial positions, while O1, O3, O5, and O7 atoms form the equatorial plane. In the anionic complexes, the N1–Cu1–N2 angle is 174.79(10)°, respectively, and is deviated from linearity. In compound **1**, the O3–Cu1–O5–C8, O3–Cu1–O7–C14,

O5–Cu1–O3–C7, and O1–Cu1–O7–C14 torsion angles are 94.7(2), −99.1(2), 99.3(2), and 99.6(2)°, respectively, indicating that two (pydc)$^{2-}$ and (pydcH)$^-$ units are almost perpendicular to each other. In compound **1**, the mean Cu–N and Cu–O bond distances are 1.932(2) and 2.186(2) Å, respectively. The Cu1–O5 and Cu1–O7 bond distances are significantly longer than other bonds which indicate a weak Jahn–Teller distortion. The extensive π–π stacking interaction between aromatic rings of pyridine-2, 6-dicarboxylate fragments, (pydc)$^{2-}$ and (pydcH)$^-$, with (AcrH)$^+$ ions with centroid–centroid distances of 3.7225(18) Å for Cg1···Cg2 (1/2 + x, 3/2 − y, 1/2 + z), 3.8985(19) Å for Cg1···Cg3 (1/2 + x, 3/2 − y, 1/2 + z), 3.5416(18) Å for Cg4···Cg2 (x, y, z) and 3.7750(19) Å for Cg4···Cg3 (x, y, z) are observed in the compound **1** [Cg1 to Cg4 are the centroids for N1/C2–C6, N3/C19, C20, C21, C26, C27, C15–19, C27 and N2/C9−C13 rings, respectively]. Therefore, another noticeable feature of the compound **1** is the presence of C=O···π stacking interactions between C=O groups and aromatic ring of (pydc)$^{2-}$ with O···π distance of 3.703(2) Å for C7−O4···Cg1 (2 − x, 1 − y, 2 − z) [Cg1 = N1/C2–C6 ring] (Fig. S2). The structure features

Table 2 Selected bond lengths [Å] and angles [°] for compounds 1–3

Compound **1**			
Cu1–N1	1.910(2)	Cu1–O1	2.112 (2)
Cu1–N2	1.953(2)	Cu1–O7	2.207(2)
Cu1–O3	2.085(2)	Cu1–O5	2.341(2)
N1–Cu1–N2	174.79(10)	O3–Cu1–O7	95.16(8)
N1–Cu1–O3	79.97(9)	O1–Cu1–O7	94.90(8)
N2–Cu1–O3	99.48(9)	N1–Cu1–O5	99.09(8)
N1–Cu1–O1	79.29(9)	N2–Cu1–O5	75.72(9)
N2–Cu1–O1	100.80(8)	O3–Cu1–O5	90.94(8)
O3–Cu1–O1	158.85(8)	O1–Cu1–O5	88.26(8)
N1–Cu1–O7	107.23(8)	O7–Cu1–O5	153.64(7)
N2–Cu1–O7	77.98(9)		
O1–Cu1–O5–C8	−106.4(2)	O3–Cu1–O7–C14	−99.1(2)
O3–Cu1–O5–C8	94.7(2)	O1–Cu1–O7–C14	99.6(2)
O7–Cu1–O1–C1	105.37(19)	O7–Cu1–O3–C7	−106.4(2)
O5–Cu1–O1–C1	−100.86(19)	O5–Cu1–O3—C7	99.3(2)
Compound **2**			
Co1–O1	2.0516(14)	O3–C6	1.270(2)
Co1–N1	2.0976(15)	O4–C6	1.232(2)
Co1–O5	2.1285(16)	O1–C5	1.268(2)
O2–C5	1.239(2)	O1–Co1–O5	88.88(6)
N1–Co1–O5	90.34(6)	C5–O1–Co1	117.11(11)
O1[i]–Co1–O1	180.00(5)	C4–N1–Co1	128.48(12)
O1[i]–Co1– N1[i]	79.12(5)	N1[i]–Co1–N1	180.0
Compound **3**			
Zn1–O1	2.0548(17)	Zn1–N1	2.0955(19)
Zn1–O5	2.2034(19)	O3 –C6	1.258(3)
O4–C6	1.240(3)	O1–C5	1.268(3)
O2–C5	1.235(3)		
O1–Zn1–O1[i]	180.00(6)	O1[i]–Zn1–N1[i]	79.84(7)
N1[i]–Zn1–N1	180.0	N1–Zn1–O5	90.57(7)
O1–Zn1–O5	89.16(7)	C5–O1–Zn1	116.03(14)

Symmetry codes: (i) $-x + 1$, $-y + 1$, $-z + 1$
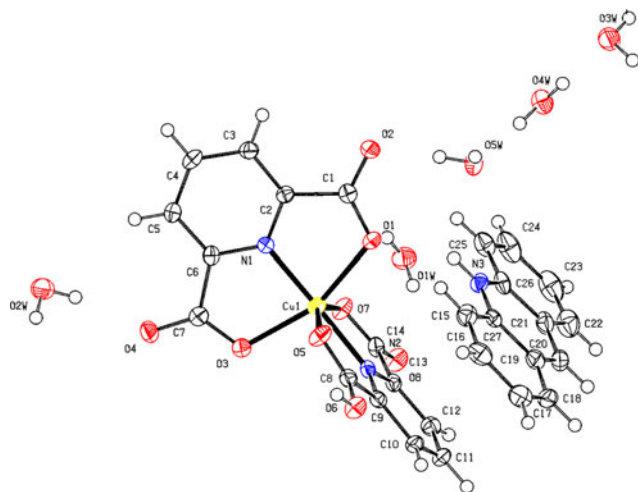
Fig. 1 Molecular structures of (AcrH)[Cu(pydc)(pydcH)]·5H$_2$O, (**1**), thermal ellipsoids are shown at 50% probability level

extensive hydrogen bonding as well distinct interactions within crystalline network. A remarkable feature in the crystal structure of the title compounds is the presence of a large number of O–H···O, N–H···O, and C–H···O hydrogen bonds (Table S1), with D···A distances ranging from 2.473(3) to 3.402(4) Å among (AcrH)$^+$, [Cu(pydc)(pydcH)]$^-$ fragment, and uncoordinated water molecules. The ranges of D−H···A angles and of the H···A and D···A distances indicate the presence of strong and weak hydrogen bonding. These interactions connect the different fragments to form 3D networks. Moreover, ion pairing, dipole–dipole, π···π, and C=O···π stacking are also effective in the packing. These interactions result in the formation of supramolecular structures. There are also uncoordinated water molecules in the molecular structures of (AcrH) [Cu(pydc)(pydcH)]·5H$_2$O, (**1**), which are linked to each
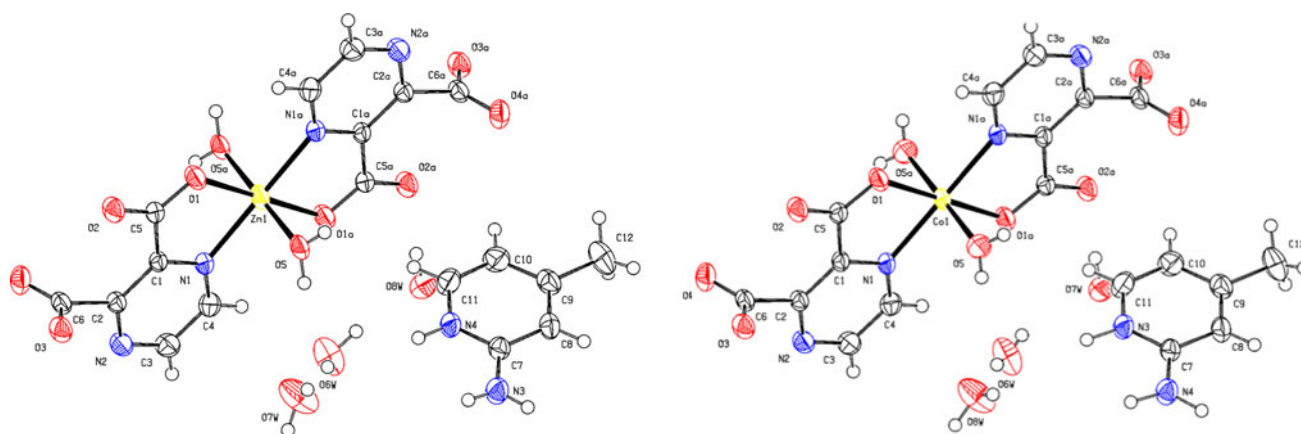
Fig. 2 Molecular structure of compounds (2-apyH)$_2$[Co(pyzdc)$_2$(H$_2$O)$_2$]·6H$_2$O, (**2**), (2-apyH)$_2$[Zn(pyzdc)$_2$(H$_2$O)$_2$]·6H$_2$O, (**3**)

other to form a cyclic water pentamer clusters by extensive hydrogen binding in the compounds [49].

Structural description of compounds 2 and 3

The results of all characterizations reveal that compounds **2** and **3** are iso-structural with the general formula (2a-4mpyH)$_2$[M(pyzdc)$_2$(H$_2$O)$_2$]·6H$_2$O; M = Co(II) and Zn(II) labeled as **2** and **3**, respectively. The structural units of **2** and **3** are built up of anionic complex fragment, [M(pyzdc)$_2$(H$_2$O)$_2$]$^{2-}$, two 2a-4mpy as cationic fragments, (2a-4mpyH)$^+$, and six crystallization water molecules. The central metal chelated by two N atoms of the pyrazine ring, two monodentate carboxylate O atoms, and two O atoms from two coordinated water molecules, forming a distorted octahedral N$_2$MO$_4$ unit. Figure 2 shows the molecular structure of compounds **2** and **3**. Where the existence of numerous hydrogen bonding, π–π stacking, C–H···π, and electrostatic interactions are outstanding. The [M(pyzdc)$_2$(H$_2$O)$_2$]$^{2-}$, linked together by classical O–H···O hydrogen bonds. The slipped or offset π–π stacking between aromatic rings of cationic moieties with centroid–centroid distance of 3.636 and 3.633 Å, N4−H6···π is 3.741 Å, N3−H7···π is 3.775 Å, and C8−H8···π is 3.580 and 3.581 Å for Co(II) and Zn(II) coordination compounds, respectively, is observable (Fig. S3). In both compounds causes further stabilization of two cationic counterparts [12]. The crystal packing of **2** along *a* axis shows arrangement of the anionic fragments by using hydrogen bonds to construct the 1D pseudo porous structure, that is, the 1D pseudo polymeric chains which resulted in the creation suitable holes for entering 2a-4mpy counter cations between respective spaces. As another interesting feature of compound **2** is presence of the cyclic $R_2^2(8)$ pattern between cationic ligand and anionic complex (Fig. S3). Increasing the number graph sets stabilizes crystalline network. In addition, the N–H···O

hydrogen bonds between dicarboxylate ligand (O3, O4) and (2a-4mpyH)$^+$ connect the anionic and cationic fragments to each other. Finally, the water molecules making various hydrogen bond networks should not be ignored in the crystal packing. Because of close similarity between compounds **2** and **3**, all of these occurrences could also be observed and explained for compound **3**.

Solution studies

The details were described in references [50–55]. The concentrations of 2a-4mpy, pyzdc, pydc, and 2-apy were 2.50×10^{-3} M, for the potentiometric pH titrations of pyzdc, 2a-4mpy, pydc, 2-apy, pyzdc-2a-4mpy, and pydc-2-apy in the absence and presence of 1.25×10^{-3} metal ions. A standard carbonate-free NaOH solution (0.095 M) was used in all titrations. The ionic strength was adjusted to 0.1 M with KNO$_3$. Before pH measuring, the system allowed to come sufficient time to equilibrium. Ligands' protonation constants, stability constants of proton transfer and their metal complexes were evaluated using the BEST program [56]. The value of $K_w = [H^+] [OH^-]$ used in calculations is similar to our previous works [50–52].

The concentrations of Acr and pydc were 3.33×10^{-3} M, for the potentiometric pH titrations of pydc, Acr, and pydc-Acr, in the absence and presence of 1.67×10^{-3} metal ions. A standard carbonate-free NaOH solution (0.097 M) in 50% dioxane–50% water (V/V) solvent was used in all titrations. The ionic strength was adjusted to 0.1 M with NaClO$_4$. The following steps were carried out similar to above. The protonation constants of pydc, Acr and stability constants of proton transfer and their metal ion complexes were evaluated using the BEST program. The value of autoprotolysis constant for 50% dioxane–50% water (v/v) solvent ($K_s = [H^+] [OH^-]$) was calculated according to the literature [56]. According to our previous work [53–55], the potentiometric study of the pydc–Acr

system was carried out in a 50% dioxane–50% water (v/v) solvent.

The fully protonated forms of pyzdc (L), 2a-4mpy (Q), pydc (L′), 2-apy (Q′), and Acr (Q″) were titrated with a standard NaOH solution in corresponding solvent order to obtain some information about protonation constant of all ligands. The protonation constants of pyzdc, pydc, 2a-4mpy, and 2-apy were calculated by fitting the volume–pH data (Fig. 3a–c), to the BEST program. The results are summarized in Table 3. Distribution diagrams for pyzdc, 2a-4mpy, and 2-apy are shown in Fig. S4a–c. The titration curve and distribution diagram for pydc in aqueous solution, pydc and Acr in a 50% dioxane–50% water (v/v) solvent were given in our previous publications [51, 54]. The titration curve and the results for pyzdc-2a-4mpy and pydc-2-apy are shown in Figs. 4a, 5a and Table 3, as well as the corresponding species distribution diagram in Fig. S5a, b. The resulting protonation constant values are in satisfactory agreement with those reported for 2-apy [57], 2a-4mpy [58], and pyzdc [59]. The observed differences between literature results and this work are due to the differences in experimental condition. The evaluation of the equilibrium constants for the reactions of pyzdc with 2a-4mpy or pydc with 2-apy in different protonation forms, were accomplished through comparison of the calculated and experimental pH profiles, obtained with the presence of pyzdc and 2a-4mpy or pydc and 2-apy [50, 53–55, 60]. It is obvious from Fig. S5a, b and Table 3 that the most abundant proton-transfer species at pH 6.4 (67.4%) and pH 2.0 (10.1%) are 2a-4mpyHpyzdc (log $K = 3.43$) and 2a-4mpyHpyzdcH$_2$ (log $K = 2.79$), respectively. The corresponding species distribution diagram for pyzdc-2-apy is

shown in Fig. S5b. It is seen that the most abundant proton-transfer species present at pH 6.2 (31.2%) and pH 3.6 (40.9%) are 2-apyHpydc (log $K = 2.56$) and 2-apyHpydcH (log $K = 2.74$), respectively.

The proton-transfer constants of pydc-Acr in a 50% dioxane–50% water (V/V) solvent was reported in our previous paper [54]. To evaluate the stoichiometry and stability of Cu^{2+}, Co^{2+}, and Zn^{2+} complexes with pyzdc-2a-4mpy, Fe^{3+}, and Cr^{3+} complexes with pydc-2apy and Cu^{2+} and Zn^{2+} with pydc-Acr proton-transfer systems in corresponding solvents, the equilibrium potentiometric pH titration profiles of pyzdc, 2a-4mpy and their 1:1 mixture, pydc [51, 52], 2-apy and their 1:1 mixture in aqueous solution and pydc, Acr and pydc-Acr in a 50% dioxane–50% water (v/v) solvent were obtained in the absence and presence of the cited metal ions. The resulting pH profiles were shown in Figs. 3a–c, 4a, 5a, S8a, b, and S11a. The titration of ligand in the presence of metal ions was stopped by observing of precipitation.

It was found that there is no reaction between 2a-4mpy and Co^{2+} and Cu^{2+} ions and very weak interaction with Zn^{2+}. The titration curves of pyzdc and pyzdc-2a-4mpy in the presence of the cited metal ions were depressed considerably. Figures 3c and 5a show that 2-apy forms relatively stable complexes with the Cr^{3+} and Fe^{3+} ions and the potentiometric titration curves pydc-2-apy mixtures are depressed considerably in the presence of the cited two metal ions. It is seen from Fig. S8b that the titration of Acr in the presence of metal ions was stopped when observed the precipitate. It was found that Acr forms relatively weak complexes with the Cu^{2+} and does not interact with Zn^{2+}, while the potentiometric titration curves of pydc and

Table 3 Overall stability and stepwise protonation constants of pyzdc, 2a-4mpy, pydc, and 2-apy and recognition constants of pyzdc with 2a-4mpy and pydc with 2-apy in aqueous solution at 25 °C and $\mu = 0.1$ M KNO$_3$

System	Stoichiometry					Log β	Equilibrium quotient K	log K	Max %	At pH
	2a-4mpy	pyzdc	2-apy	pydc	h					
pyzdc-2a-4mpy	0	1	0	0	1	4.85	–	4.85	97.7	3.0
	0	1	0	0	2	5.83	–	0.98	8.5	2.0
	1	0	0	0	1	7.95	–	7.95	99.9	3.5–4.9
	1	0	0	0	2	8.36	–	0.41	2.4	2.0
	1	1	0	0	1	11.38	[2a-4mpypyzdcH]/[2a-4mpyH][pyzdc]	3.43	67.4	6.4
	1	1	0	0	3	16.57	[2a-4mpypyzdcH$_3$]/[2a-4mpyH$_2$][pyzdcH]	3.36	10.1	2.0
							[2a-4mpypyzdcH$_3$]/[2a-4mpyH][pyzdcH$_2$]	2.79		
Pydc-2-apy	0	0	1	0	1	5.04	–	5.04	91.1	3.7
	0	0	1	0	2	7.45	–	2.41	69.0	2.0
	0	0	1	0	3	8.24	–	0.79	2.2	2.0
	0	0	0	1	1	6.99	–	6.99	99.5	4.1–4.5
	0	0	0	1	2	8.61	–	1.62	29.4	2.0
	0	0	1	1	1	9.55	[2-apypydcH]/[2-apyH][pydc]	2.56	31.2	6.2
	0	0	1	1	2	14.77	[2-apypydcH$_2$]/[2-apyH][pydcH]	2.74	40.9	3.6

Fig. 3 Potentiometric titration curves of pyzdc (**a**), 2a-4mpy (**b**), and 2-apy (**c**) in the absence and presence of M^{n+} ions with NaOH 0.095 M in aqueous solution at 25 °C and $\mu = 0.1$ M KNO_3; M = Co^{2+}, Cu^{2+}, Zn^{2+}, Cr^{3+}, and Fe^{3+}
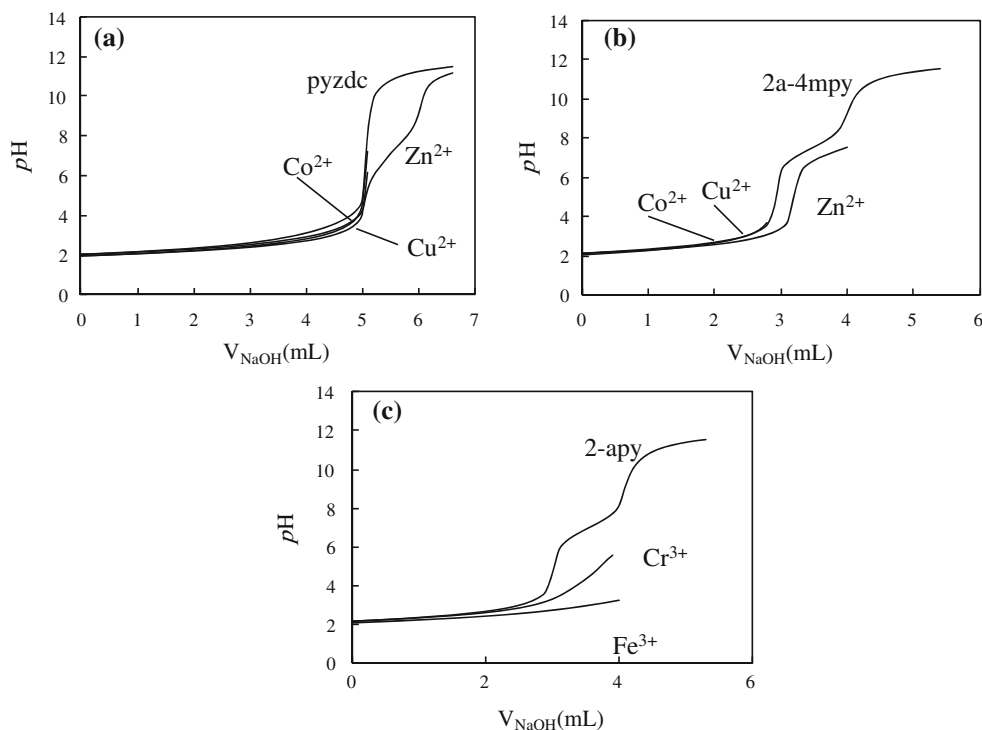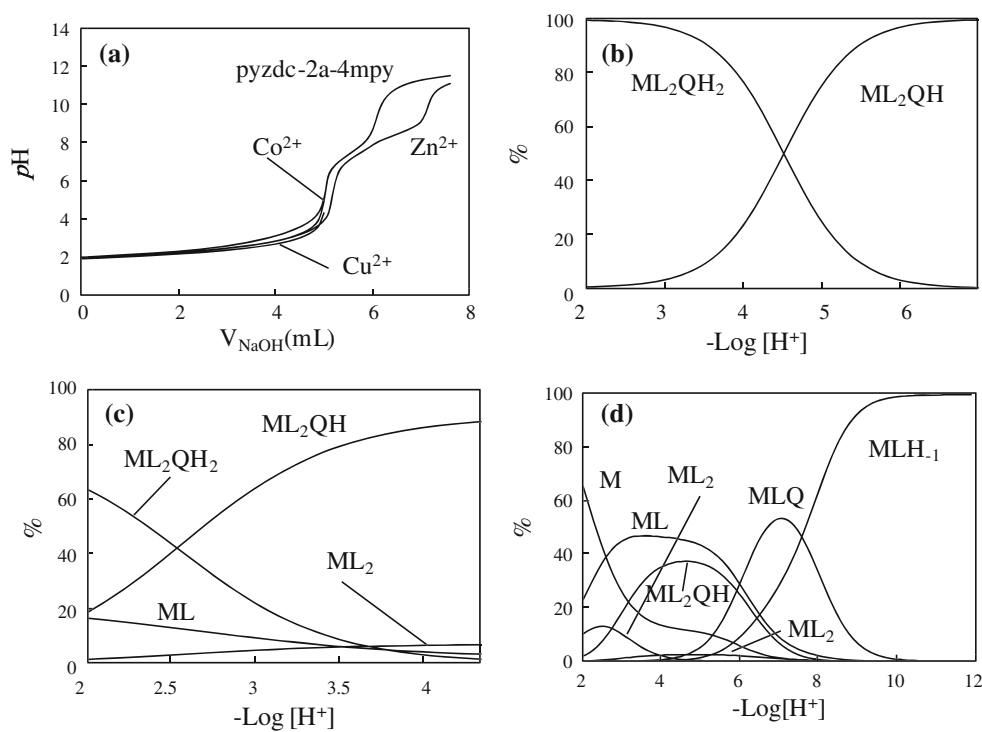
Fig. 4 Potentiometric titration curves of pyzdc + 2a-4mpy in the absence and presence of M^{2+} ions with NaOH 0.095 M in aqueous solution at 25 °C and $\mu = 0.1$ M KNO_3, M = Co^{2+} and Cu^{2+} (**a**) and distribution diagrams of pyzdc(L)/2a-4mpy(Q)/M ternary systems. M = Co^{2+} (**b**), Cu^{+2} (**c**), and Zn^{2+} (**d**)

pydc–Acr mixtures are depressed considerably in the presence of the metal ions. The extent of depression obviously depends both on the stoichiometries of resulting complexes and the ability of the metal ions to bind the ligand components.

The cumulative stability constants of $M_mL_lQ_qH_h$, β_{mlqh}, were defined in previous publications [50, 51]. M, L, Q, and H are metal ions, pyzdc or pydc, 2a-4mpy, 2-apy or Acr and proton, respectively, and m, l, q, and h are the stoichiometric coefficients. The cumulative stability constants were evaluated by fitting the corresponding pH titration curves to the BEST program. The resulting values for the most likely complexed species in aqueous solutions

Fig. 5 Potentiometric titration curves of pydc^{2+}-apy in the absence and presence of M^{3+} ions with NaOH 0.095 M in aqueous solution at 25 °C and $\mu = 0.1$ M KNO$_3$, M = Cr^{3+} and Fe^{3+} (**a**) and distribution diagrams of pydc(L′)/2-apy (Q′)/M ternary systems. M = Cr^{3+} (**b**), and Fe^{3+} (**c**)
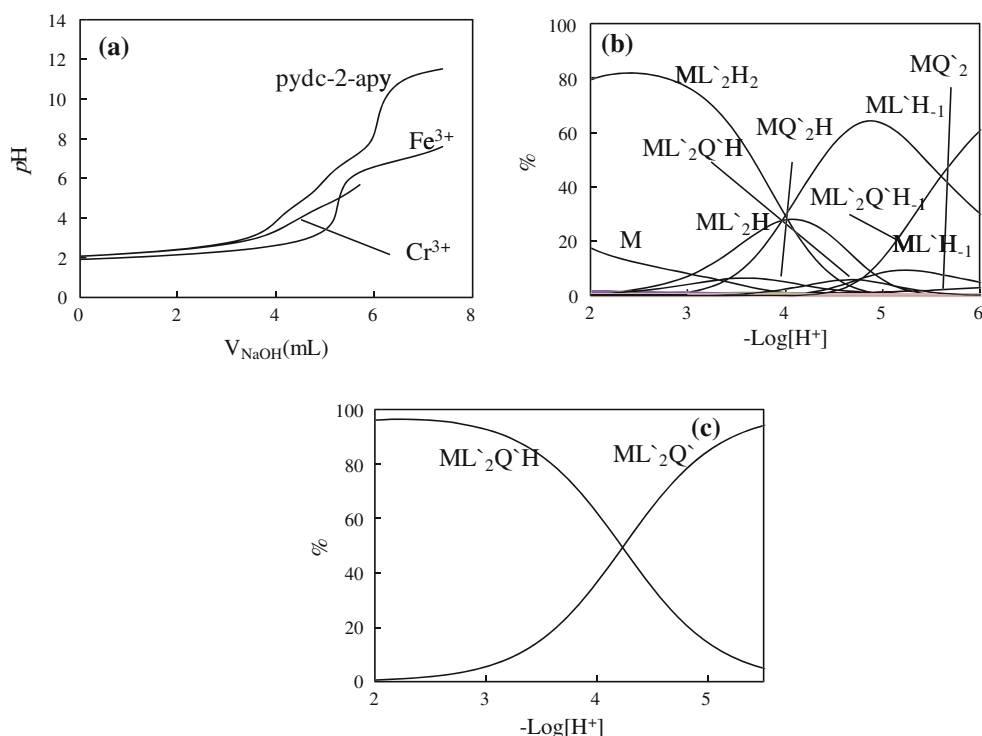
Table 4 Overall stability constants of Acr/pydc/M^{2+} ($q/l/m$) binary and ternary systems in a 50% dioxane–50% water (v/v) solvent at 25 °C and $\mu = 0.1$ M NaClO$_4$

System	m	l	q	h	Log β	Max %	At pH
Cu-pvdc	1	1	0	0	9.92	26.4	2.0
	1	2	0	0	16.78	99	>7.3
	1	2	0	1	21.13	77	3.4
	1	2	0	2	23.43	44.8	2.0
Zn-pydc	1	1	0	0	9.14	78.2	2.3
	1	2	0	0	14.21	93	7.7
	1	2	0	1	18.83	61.6	3.8
Cu-Acr	1	0	2	0	5.47	36.7	5.2
	1	0	1	−1	−2.54	94.4	7.3
	1	0	1	−2	−11.4	99.8	>11.3
Cu-pydc-Acr	1	2	1	1	26.84	93.6	5.8
	1	2	1	2	31.10	94.4	2.5
Zn-pydc-Acr	1	2	1	1	25.61	98	6.3
	1	2	1	2	29.82	68.8	3.5
	1	2	2	3	33.18	Negligible	–
	1	2	2	4	40.55	69.6	2.0

and 50% dioxane–50% water (v/v) solvent were shown in Tables 2S and 4 respectively, as well as the corresponding distribution diagrams were shown in Figs. 4, 5, S6, S7, S9, S10, and S11b, c.

Figure S6d and Table S2 are similarly for 2a-4mpy-Zn system, the most likely species are ZnQ and ZnQH$_{-1}$.

From Fig. S6 and Table S2 for pyzdc (L), as a ligand, the most likely species for Co^{2+} are CoL, CoLH, CoL$_2$, and Co$_2$L; for Cu^{2+} are CuL and CuL$_2$; for Zn^{2+} are ZnL, ZnL$_2$, ZnL$_2$H, and ZnLH$_{-1}$. The observed species and their corresponding stability constants of pydc-Cr and pydc-Fe systems were given in our previous publications [51, 52]. Figure S7a, b and Table S2 show for 2-apy-M system, the most likely species for Cr^{3+} are CrQ′, CrQ′H, CrQ′$_2$, CrQ′$_2$H, CrQ′$_2$H$_2$, and CrQ′H$_{-1}$, for Fe^{3+} are FeQ′H and FeQ′$_2$. As it is obvious from Fig. S10 and Table 4 in the case of pydc(L), as ligand, the most likely species for Cu^{2+} are CuL, CuL$_2$, CuL$_2$H, and CuL$_2$H$_2$ and for Zn^{2+} are ZnL, ZnL$_2$, and ZnL$_2$H. Figure S10 and Table 4 show for Acr–M system, for Zn^{2+} was not found considerable interaction with Acr, the most likely species for Cu^{2+} are CuQ″$_2$, CuQ″H$_{-1}$, and CuQ″H$_{-2}$.

Figures 4 and 5 and Table S2 revealed the formation of a variety of ternary complexes with the abovementioned cations and the proton-transfer system at different ranges of pH. The predominant species for pyzdc-2a-4mpy-Cu^{2+} are CuL$_2$QH (at pH 4.3) and CuL$_2$QH$_2$ (at pH 2.0) for pyzdc-2a-4mpy-Co^{2+} are CoL$_2$QH (at pH 6.98) and CoL$_2$QH$_2$ (at pH 2.0) for pyzdc-2a-4mpy-Zn^{2+} are ZnLQ (at pH 7.0) and ZnL$_2$QH (at pH 4.7). Similarly for pydc-2-apy-Cr^{3+} are CrL′$_2$Q′H (at pH 4.7), CrL′$_2$Q′H2 (at pH 4.1) and CrL′$_2$Q′H$_{-1}$ (at pH 6.0) for, pydc-2-apy-Fe^{3+} are FeL′Q′ (at pH >5.5), FeL′Q′H (at pH >5.5), FeL′$_2$Q′ (at pH 5.5), and FeL′$_2$Q′H (at pH 2.2).

Figure S11b, c and Table 4 revealed the formation of a variety of ternary complexes between the abovementioned cations and the proton-transfer system at different ranges of pH. The predominant species for Cu^{2+} are $CuL_2Q''H$ (at pH 5.8) and $CuL_2Q''H_2$ (at pH 2.5) and for Zn^{2+} are $ZnL_2Q''H$ (at pH 6.3), $ZnL_2Q''H_2$ (at pH 3.5) and $ZnLQ''_2H_4$ (at pH 2). It is interesting to note that the stoichiometries of the some of the most abundant ternary complexes, existing in aqueous solution and a 50% dioxane–50% water (v/v) solvent, are the same or very similar to those reported for the corresponding isolated complexes in the solid state.

Computational approach

All calculations have been performed by using gradient-corrected density functional theory with the B3LYP functional [61] as implemented in the Gaussian 98 software package [62]. The 6-31+G(d,p) basis set was employed except for the metal atoms, in which the LANL2DZ [63] basis set was used including effective core potential functions. Geometries of the complexes were fully optimized, and were used to calculate the natural electron population, i.e., the natural charge for each atom and molecular orbitals of the complexes by natural bond orbital (NBO) analysis. For increasing accuracy of calculations, one sp diffuse function, d and p polarization functions were included. Recently published work by our research group [53–55], showed that B3LYP level may results in good data about proton-transfer compound. Hence, in this work, we have applied above mentioned level, too.

Optimized structure of [Cu(pydc)(pydcH)]⁻ anion

Geometrical parameters of the optimized structure of the $[Cu(pydc)(pydcH)]^-$ anion obtained by B3LYP quantum chemical calculations are reported in Table 5. The $[Cu(pydc)(pydcH)]^-$ anion consists of $(pydc)^{2-}$ and $(pydcH)^-$ ligands which bond to metal perpendicularly to each other as shown in the Fig. 1. For comparison, the free $(pydc)^{2-}$ and $(pydcH)^-$ ligands have been optimized at the B3LYP level using standard basis set 6-31+g(d, p) which is also included in the Table 5. The optimized geometry confirms that the C–O(bonded) bond length of $(pydc)^{2-}$ and $(pydcH)^-$ ligands in its complex form has been increased compared with the free ligands. Also, in the complex form this bond is longer than C=O(free) bond. The evidence shows that C–O(bonded) is weakened on formation of complex, while C=O(free) converted to double bond. The obtained results from HOMO and LUMO investigations may be used for analyzing of observed bond lengths. Schematic representation of HOMO and LUMO orbitals of the free $(pydc)^{2-}$ ligand in Fig. 6, demonstrate

Table 5 Selected experimental and B3LYP calculated geometry parameters of the $(pydc)^{2-}$ and $(Hpydc)^-$ ligands together with the $[Cu(pydc)(Hpydc)]^-$ complex

Bond	Complex		Ligand	
	Calculated	Experimental	pydc	Hpydc
Cu1–N2	2.112	1.953(2)	–	–
Cu1–N1	1.950	1.910(2)	–	–
Cu1–O5	2.761	2.341(2)	–	–
Cu1–O7	2.177	2.207(2)	–	–
Cu1–O1	2.066	2.112(2)	–	–
Cu1–O3	2.065	2.085(2)	–	–
C13–N2	1.338	1.347(3)	–	1.340
C2–N1	1.333	1.335(3)	1.348	–
C8–O5	1.211	1.228(3)	–	1.212
C14–O7	1.263	1.254(3)	–	1.247
C7–O3, C1–O1	1.289	1.279(3), 1.281(3)	1.252	–
C8–O6	1.362	1.294(3)	–	1.379
C14–O8	1.245	1.260(3)	–	1.264
C7–O4, C1–O2	1.237	1.245(3), 1.235(3)	1.252	–
O6–H1	0.971	0.82	–	0.970

higher MO distributions around oxygen atoms in HOMO and pyridine ring atom in LUMO frontal orbitals. However, the free $(pydcH)^-$ ligand includes higher MO distributions around oxygen atoms of COO^- group in HOMO and nitrogen atom and oxygen atoms of COOH group in LUMO frontal orbitals (Fig. 7). The HOMO orbital of
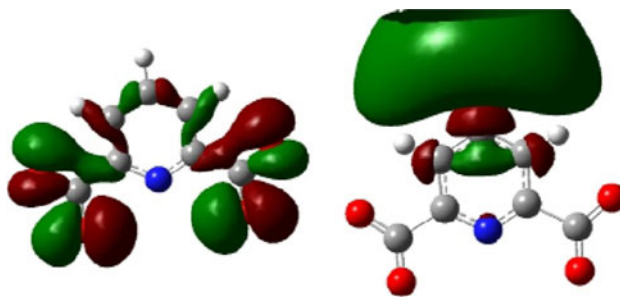

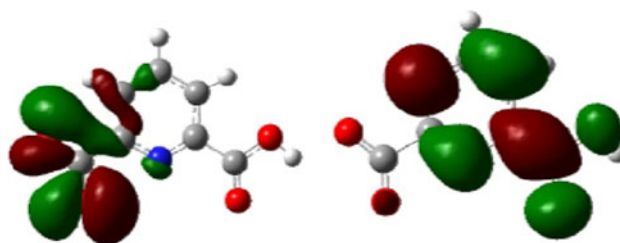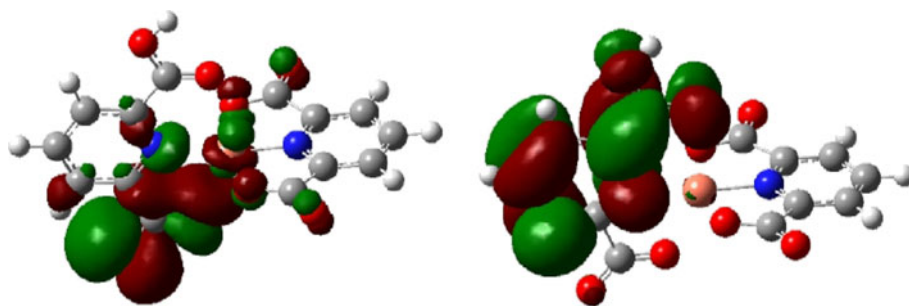**Fig. 6** The 3D representation of HOMO and LUMO frontal orbitals of free $(pydc)^{2-}$ ligand

Fig. 7 The 3D representation of HOMO and LUMO frontal orbitals of free $(pydcH)^-$ ligand

Fig. 8 The 3D representation of HOMO and LUMO frontal orbitals of [Cu(pydc)(pydcH)]⁻ anion

complex (Fig. 8) shows the strong overlapping of the electron clouds have been done between d_{z^2} atomic orbital of Cu metal with p_z orbital of O1 and O3 atoms in (pydc)²⁻ ligand and O7 atom of COO⁻ group in (pydcH)⁻ ligand. The LUMO orbital of complex (Fig. 8) locates on nitrogen atom and oxygen atoms of COOH group in (pydcH)⁻ ligand. According to the theoretical data, the C1–O1 and C7–O4 bonds in the title complex have been strengthen than free pydc ligand (0.037 Å). The reason is atomic orbitals of O3 and O1 are engaged in HOMO orbitals, but C8–O5 bond was not altered. Since, electronic cloud of O5 atom did not participate in HOMO orbital, so, Cu1–O5 bond is longer than other Cu–O bonds, which indicates that this bond is the weakest one. Inversely, much more overlapping of atomic orbitals of O3 and O1 in HOMO orbitals causes the related bonds to be strengthen. The NBO studies verifies above evidences. The natural charge of O5 atom has been decreased to −0.258 in the complex, from −0.473 for the free (pydcH)⁻ ligand (about 0.215), however, the decreasing of natural charge of O1 and O3 atoms is greater −0.230 compared to −0.601 in the free (pydc)²⁻ ligand. These results verify that in the complex formation process, the electron density of O5 atom shifts to Cu atom greater than O1 and O3 atoms. The Cu1–N1 bond in (pydc)²⁻ ligand is shorter and strengthen than Cu1–N2 bond in (pydcH)⁻ ligand. The more charge density on N2 atom than N1 atom (−0.183 and −0.170, respectively) support this case.

Optimized structures of the [M(pyzdc)₂(H₂O)₂]²⁻ anion complexes, M = Cu(II) and Zn(II)

Optimized geometries of the octahedral complexes according to the Fig. 2 and Ref. 24 and their B3LYP obtained geometrical parameters were listed in Table S3. The [ML₂(H₂O)₂] complexes consist of two bidentate L ligands, which are in the same plane. The complexes have an inversion center and two water ligands occupying the axial positions of the octahedral complexes. The calculated values are well in agreement with the experimental results. The natural charges and electron configurations on the atoms of complexes were listed in Table S4. Electron

donation of O atoms of the ligand is more than of the H₂O. This causes a longer metal–O bond for the H₂O ligands and more electron density on the O5 atoms in comparison with the O1(Zn) and O2(Cu) atoms. Coordination of the O1 and O2 atoms causes electron deficiency on the C5(Zn) and C1(Cu) atoms. Electronic clouds on the O1(Cu) and O2(Zn) atoms are shifted to the C5–O2(Zn) and C1–O1 bonding(Cu) regions, so increase the strengths of these bonds and decrease the electron density on the O2(Zn) and O1(Cu) atoms. Electron density of the HOMO is more localized on the free carboxylate oxygen atoms of the Zn complex, especially on the O3 and O4 which makes them more negative. In Cu complex, the HOMO is more localized on the non-bonded O1 atom, which causes more negative charge on these atoms in comparison with the Zn complex (Table S4). For Zn complex, electron density of the LUMO is more localized on the aromatic rings. For Cu complex, this orbital is more localized on the $d_{x^2-y^2}$ (orbital of the metal) and p_z (orbital of the coordinated atoms of the L ligand) (Fig. 9). The HOMO → LUMO electron transferring decreases the positive charge on Cu atom.

Conclusion

In this article, we have synthesized three new coordination compounds involving pyridine-2,6-dicarboxylic acid and 1,4-prazin-2,3-dicarboxylic acid which characterized by spectral method (IR), elemental analyses, TGA, and single crystal X-ray diffraction techniques. The van der Waals interactions especially hydrogen bonding (such as O–H···O and N–H···O) and slipped or offset π···π, N–H···π, C–H···π, and C=O···π stacking interactions play essential roles in creation and stabilization of their 3D supramolecular networks. Also, we try to compare the present structures with similar compounds which have been made previously. Potentiometric and DFT studies are also carried out.

Supplementary material

CCDC No. 805365, 769042, and 769043 for the supplementary crystallographic data for **1** to **3** coordination
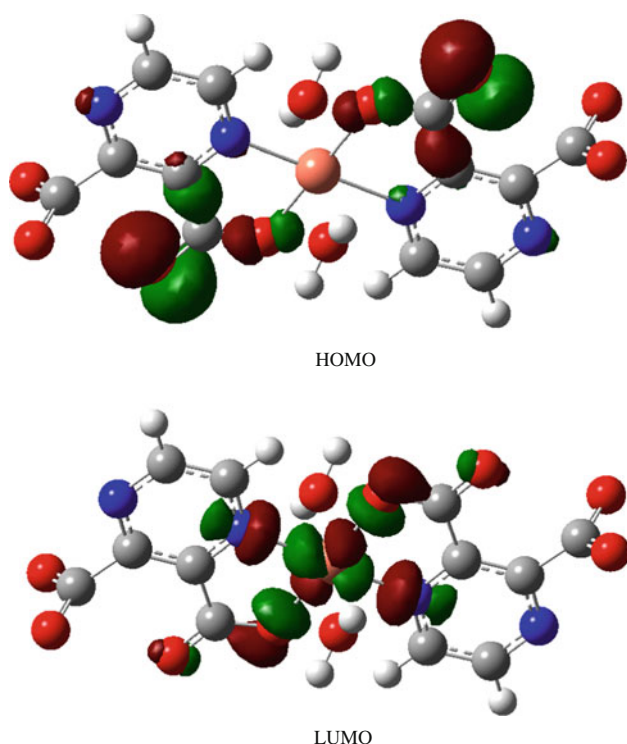
HOMO

LUMO

Fig. 9 The 3D representation of HOMO and LUMO frontal orbitals of the Cu complex

compounds. These data can be obtained free of charge via http://www.ccdc.cam.ac.uk/conts/retrieving.html, or from the Cambridge Crystallographic Data Centre, 12 Union Road, Cambridge CB2 1EZ, UK; fax: (+44) 1223-336-033; or email: deposit@ccdc.cam.ac.uk.

References

1. Wang CJ, Wang YY, Liu JQ, Wang H, Shi QZ, Peng SM (2009) Inorg Chim Acta 362:543
2. Çolak AT, Yeşilel OZ, Hökelek T, Şahin E (2008) Struct Chem 19:285 and Refs. [6–29] therein
3. Chakraborty J, Shaikh N, Mayer-Figge H, Sheldrick WS, Vojtíšek P, Banerjee P (2007) Struct Chem 18:157
4. Uçar I, Bulut I, Bulut A, Karadag A (2009) Struct Chem 20:825 and Refs. [8, 10, 14, 16, 17, 19, 20, 21] therein
5. Dale SH, Elsegood MRJ, Coombs AEL (2004) Cryst Eng Commun 59:328
6. Eddaoudi M, Moler DB, Li H, Chen B, Reineke TM, O'keeffe M, Yaghi OM (2001) Acc Chem Res 34:319
7. Shi Q, Zhang S, Wang Q, Ma H, Yang G, Sun WH (2007) J Mol Struct 837:185
8. Moghimi A, Moosavi SM, Kordestani D, Maddah B, Shamsipur M, Aghabozorg H, Ramezanipour F, Kickelbick G (2007) J Mol Struct 828:38
9. Vaidhyanathan R, Natarajan S, Rao CNR (2002) J Mol Struct 608:123
10. Devereux M, McCann M, Leon V, McKee V, Ball RJ (2002) Polyhedron 21:1063
11. Ene DC, Tuna F, Fabelo O, Ruiz-Pérez C, Madalan MA, Roesky WH, Andruh M (2008) Polyhedron 27:574
12. Janiak C (2000) J Chem Soc Dalton Trans 3885
13. Beatty AM (2003) Coord Chem Rev 246:131
14. Braga D, Maini L, Paganelli F, Tagliavini E, Casolari S, Grepioni F (2001) J Organomet Chem 609
15. Eppel S, Bernstein J (2008) Acta Cryst B 64:50
16. Eshtiagh-Hosseini H, Yousefi Z, Mirzaei M (2009) Acta Cryst E65:o2816
17. Eshtiagh-Hosseini H, Yousefi Z, Mirzaei M, Chen YG, Shokrollahi A, Aghaei R (2010) J Mol Struct 973:1
18. Eshtiagh-Hosseini H, Aghabozorg H, Mirzaei M, Amini MM, Chen YG, Shokrollahi A, Aghaei R (2010) J Mol Struct 973:180
19. Eshtiagh-Hosseini H, Hassanpoor A, Alfi N, Mirzaei M, Fromm KM, Shokrollahi A, Gschwind F, Karami E (2010) J Coord Chem 63:3175
20. Eshtiagh-Hosseini H, Yousefi Z, Shafiee M, Mirzaei M (2010) J Coord Chem 63:3187
21. Eshtiagh-Hosseini H, Necas M, Alfi N, Mirzaei M (2010) Acta Cryst E 66:m1320
22. Eshtiagh-Hosseini H, Alfi N, Mirzaei M, Marek N (2010) Acta Cryst E66:o2810
23. Eshtiagh-Hosseini H, Aghabozorg H, Mirzaei M (2010) Acta Cryst E66:m882
24. Eshtiagh-Hosseini H, Gschwind F, Alfi N, Mirzaei M (2010) Acta Cryst E66:m826
25. Eshtiagh-Hosseini H, Hassanpoor A, Mirzaei M, Salimi AR (2010) Acta Cryst E66:o2996
26. Eshtiagh-Hosseini H, Hassanpoor A, Canadillas-Delgado L, Mirzaei M (2010) Acta Cryst E66:o1368
27. Eshtiagh-Hosseini H, Hassanpoor A, Mirzaei M, Szymanska-Buzar T, Kochel A (2011) Acta Cryst E67:m455
28. Eshtiagh-Hosseini H, Mahjoobizadeh M, Mirzaei M (2010) Acta Cryst E66:o2210
29. Eshtiagh-Hosseini H, Mahjoobizadeh M, Mirzaei M, Fromm KM, Crochet A (2010) Eur J Chem 1:179
30. Aghabozorg H, Manteghi F, Sheshmani S (2008) J Iran Chem Soc 5:184
31. Mirzaei M, Aghabozorg H, Eshtiagh-Hosseini H (2011) J Iran Chem Soc (in press)
32. Tabatabaee M, Aghabozorg H, Attar Gharamaleki J, Sharif AM (2009) Acta Cryst E 65:m473
33. Aghabozorg H, Sadrkhanlou E, Soleimannejad J, Adams H (2007) Acta Cryst E 63:m1760
34. Soleimannejad J, Aghabozorg H, Sheshmani S (2010) Acta Cryst E 66:m411
35. Aghabozorg H, Nemati A, Derikvand Z, Ghadermazi M (2007) Acta Cryst E 63:m2921
36. Aghabozorg H, Ghadermazi M, Zabihi F, Nakhjavan B, Soleimannejad J, Sadr-khanlou E, Moghimi A (2008) J Chem Crystallogr 38:645
37. Aghabozorg H, Roshan L, Firoozi N, Bagheri S, Ghorbani Z, Kalami S, Mirzaei M, Shokrollahi A, Ghaedi M, Aghaei R, Ghadermazi M (2010) Struct Chem 21:701
38. Yeşilel OZ, Mutlu A, Büyükgüngör O (2009) Polyhedron 28:437
39. Li XH, Shi Q, Hu ML, Xiao HP (2004) Inorg Chem Commun 7:912
40. Mao L, Rettig SJ, Thompson RC, Trotter J, Xia S (1996) Can J Chem 74:433

41. Wang FQ, Zheng XJ, Sun YX (2009) Bull Korean Chem Soc 30:264
42. Yin H, Liu SX (2007) Polyhedron 26:3103
43. Bruker, APEX II software package, v. 1.27 (2005) Bruker molecular analysis research tool. Bruker AXS, Madison, WI
44. Stoe & Cie (2005) X-AREA. Stoe & Cie, Darmstadt
45. Sheldrick GM (2008) Acta Cryst A 64:112
46. Sheldrick GM, SADABS, v. 2.03 (2003) Bruker/Siemens area detector absorption correction program. Bruker AXS, Madison
47. Bruker, SAINT, v. 6.2 (2001) Data reduction and correction program. Bruker AXS, Madison
48. Sheldrick GM, SHELXTL, v. 6.12 (2001) Structure determination software suite. Bruker AXS, Madison
49. Aghabozorg H, Eshtiagh-Hosseini H, Salimi AR, Mirzaei M (2010) J Iran Chem Soc 72:89
50. Aghabozorg H, Sadr-Khanlou E, Shokrollahi A, Ghaedi M, Shamsipur M (2009) J Iran Chem Soc 6:55
51. Aghabozorg H, Ramezanipour F, Soleimannejad J, Sharif MA, Shokrollahi A, Shamsipur M, Moghimi A, Attar Gharamaleki J, Lippolis V, Blake AJ (2008) Polish J Chem 82:487
52. Aghajani Z, Aghabozorg H, Sadr-Khanlou E, Shokrollahi A, Derki S, Shamsipur M (2009) J Iran Chem Soc 6:373
53. Aghabozorg H, Manteghi F, Ghadermazi M, Mirzaei M, Salimi AR, Shokrollahi A, Derki S, Eshtiagh-Hosseini H (2009) J Mol Struct 919:381
54. Mirzaei M, Eshtiagh-Hosseini H, Lippolis V, Aghabozorg H, Kordestani D, Shokrollahi A, Aghaei R, Blake AJ (2011) Inorg Chim Acta 370:141
55. Eshtiagh-Hosseini H, Aghabozorg H, Mirzaei M, Beyramabadi SA, Eshghi H, Morsali A, Shokrollahi A, Aghaei R (2011) Spectrochim Acta 78A:1392
56. Martell AE, Motekaitis RJ (1992) Determination and use of stability constants, 2nd edn. VCH, New York
57. Joshaghani M, Sotodehnejad M (2003) Iran J Chem Chem Eng 22:17
58. Angyl SJ, Angyal CL (1952) J Chem Soc 1461
59. Wenkin M, Devillers M, Tinant B, Declercq JP (1997) Inorg Chim Acta 258:113
60. English JB, Martell AE, Motekaitis RJ, Murase I (1997) Inorg Chim Acta 258:183
61. Becke AD (1993) J Chem Phys 98:5648
62. Frisch MJ et al (1998) Gaussian 98, revision A7. Gaussian, Inc., Pittsburgh, PA
63. Hay PJ, Wadt WR (1985) J Chem Phys 82:299